Surface structure determination via a transform-deconvolution method

Uzi Landman and D. L. Adams

Xerox Corporation, Rochester Research Center, Webster, New York 14580
(Received 8 August 1973)

A fast direct-transform method for the determination of surface structures from low-energy-electron diffraction (LEED) intensity data is presented. Basic principles of a proper transform construction and its applications are discussed and demonstrated. The effects of data truncation is studied and a deconvolution procedure for extraction of accurate structural information from the transform is described. Results of a complete surface structure determination of Ni(100) by application of the method to experimental data are discussed.

I. INTRODUCTION

Basic to studies of physical processes occurring on solid surfaces is the understanding of the geometric and electronic structure of the outermost few atomic layers of the solid. Of particular importance is the geometrical structural information since it is an elementary essential for the construction of physical models of surface phenomena. Determination of surface structures from low-energy-electron diffraction (LEED) experiments requires analysis of the angular distribution and intensities of diffracted beams (diffraction patterns and intensity-voltage profiles). The customary analysis of LEED intensity measurements consists of attempts to fit experimental data via model calculations.[1-3] The high degree of uncertainty in the results derived by the above methods originates from an incomplete description of the physical phenomena associated with the diffraction of low-energy electrons and in the unavoidable failure to test *all* the possible structures of the system.

The technique presented in this paper consists of *direct transform analysis* of experimental data which avoids to a large extent the above uncertainties along with a significant reduction in computational time and storage. In order to demonstrate the principles and applications of our transform method for surface structure determination, we employ intensities calculated on the basis of kinematical diffraction,[1] application of the transform method to the analysis of real data is also included.

The construction and characteristics of the transform method applied to LEED with particular reference to the finite extent of the data, and physical interpretation, are discussed in Sec. II. In Sec. III we present structural determination of the (100) face of Ni, based on transform analysis of the experimental data of Demuth and Rhodin.[4]

II. DIRECT TRANSFORM TECHNIQUE

A. Transform Construction

As an introduction to the formulation of the direct transform method for LEED it is instructive to briefly review the construction of the Patterson function used in x-ray structure analysis, which is defined as[5]

$$P(x,y,z)=\frac{1}{V}\sum_{h,k,l=-\infty}^{\infty} I_{hkl}\exp[2\pi i(hx+ky+lz)], \quad (1)$$

where I_{hkl} is the intensity of the (hkl) diffracted beam, and V is the volume of the sample. Due to the kinematical elastic nature of x-ray diffraction (in the absence of anomalous dispersion) it follows that the Patterson function $P(\mathbf{R})$ can be expressed as the autocorrelation of charge densities

$$P(\mathbf{R})=\int \rho(\mathbf{r})\rho(\mathbf{r}+\mathbf{R})d^3r. \quad (2)$$

The expression in Eq. (1) can be further simplified (in the absence of anomalous dispersion) through the application of Friedel's law[6] yielding a *real* cosine transform of the diffracted intensities[6] rather than the complex exponential transformation in Eq. (1).

In constructing a transform appropriate for surface structure analysis, the nature of the LEED process dictates certain modifications to the Patterson function as used in x-ray studies. Characteristic to low-energy-electron diffraction is the dynamical nature of the scattering process and the inelastic collision damping of the electron-beam propagation in the direction normal to the surface.[1] Since momentum is conserved in the plane parallel to the surface but not in the normal direction, the diffracted intensities are characterized by discrete (hk) Miller indices of the surface net and the continuous variable S, the momentum transfer in the normal direction. This variable is constrained to positive values due to the half-space nature of low-energy-electron diffraction measurements in which only back-scattered electrons are detected.

These considerations lead us to the following formulation of the transform

$$P^M(x,y,z)=\sum_{h,k=-\infty}^{\infty}\int_0^{\infty} dS I_{hk}(S) \times\exp[2\pi i(hx+ky)]\exp[2\pi iSz]. \quad (3)$$

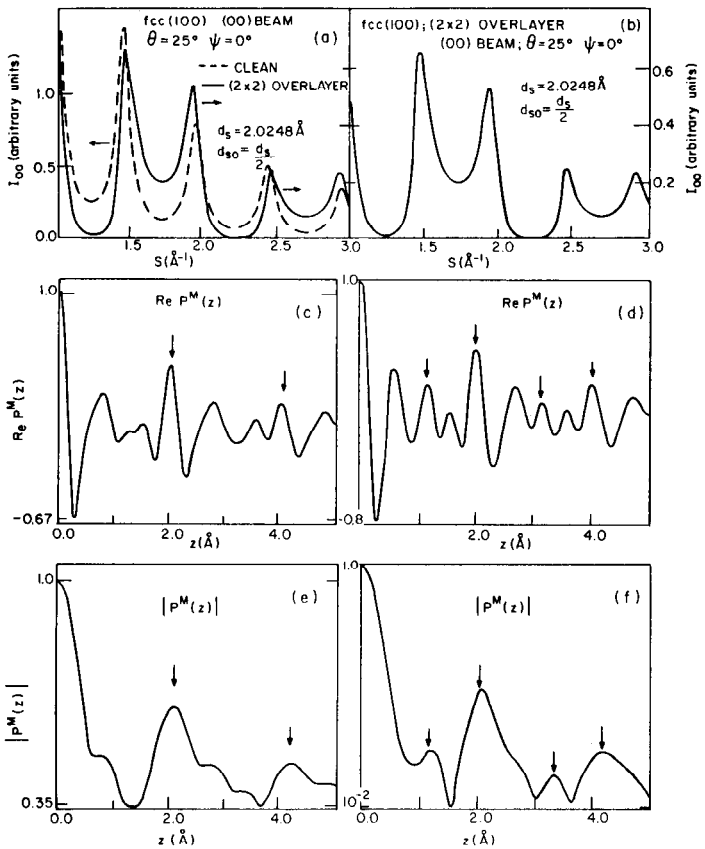

FIG. 1. (a)–(b) Kinematical intensity profiles of the (00) diffracted beam from the (100) face of an fcc clean substrate material (dashed) and in the presence of a (2×2) overlayer (solid) located at a vertical distance $d_{s0}=d_s/2$ where d_s is the layer spacing in the substrate. The profiles are presented as a function of the normal momentum transfer, S, for incidence angular parameters $\theta=25°$ and $\psi=0°$, mean free path, $\lambda_{ee}=6$ Å, an inner potential $V_0=15$ eV and scattering phase shifts $\delta_s=\pi/2$ and $\delta_o=\pi/8$ for substrate and overlayer ion-cores, respectively. The two profiles differ in relative intensities but do not exhibit significant shifts in the location of peaks. (c) The real part of the transform projection, $P^M(z)$, normalized to unity, for the clean intensity profile [dashed curve in 1(a)]. Peaks occurring at about the expected values of the layer spacing (d_s) are marked by vertical arrows. The occurrence of data-truncation peaks (Gibbs oscillations) and the negative values for part of the transform should be noted. (d) The real part of the transform projection, $P^M(z)$, normalized to unity, for the overlayer intensity profile [solid curve in (a) and (b)]. Peaks occur as expected at $\sim n(d_s/2)$ for $n=0$, 1, 2, 3, ..., (marked by vertical arrows) along with spurious peaks which are due to data truncation. Peaks due to the presence of the overlayer [missing in (c)] occur for odd values of n. (e)–(f) Modulus of the transform projection for the clean (e) and overlayed (f) cases. Expected peaks (vertical arrows) in (e) and (f) occur at positions corresponding to those in (c) and (d), respectively, with marked shifts of the $2d_s$ peak in (e) and the $3(d_s/2)$ and $2ds$ peaks in (f). These shifts are suppressed when the range of momentum transfer of the intensity profiles is extended. Compared to the corresponding real part of the transform, those in (e) and (f), exhibit less oscillations caused by data truncation. This is mainly due to the cancellation of these oscillation between the real and imaginary components of the transform which are phase shifted.

Unlike the x-ray case, this transform does not reduce to a real cosine transform since Friedel's law is not obeyed due to inelastic collision damping. (In recent publication, Clarke *et al.*[7] used a real cosine transform for the analysis of LEED data. We emphasize the lack of *a priori* justification for this procedure for surface structure analysis. In addition, these authors fail to treat the problem of data truncation which we discuss further in Sec. C.)

B. Use of Projections and Sections in Structure Determination

The transformation given in Eq. (1) defines a three-dimensional vector space.[6] Each point (x,y,z) in this space represents a position vector $\mathbf{R}\equiv(x,y,z)$ connecting two scattering centers, translated to an arbitrary common origin. In most cases that we have studied, structure determination can be based on the analysis of projections and sections of the transform rather than the full three-dimensional function.[5–6] Of particular use in surface structure analysis is the one-dimensional projection of the transform in Eq. (3), denoted by $P^M(z)$

$$P^M(z)=\int_0^\infty dSI_{00}(S)\exp[2\pi iSz], \tag{4}$$

where I_{00} is the intensity of the specularly diffracted electron beam. This projection is used in the determination of layer spacings as demonstrated below. Determination of layer registry is achieved by the analysis of sections of the P^M transform, denoted by $P^M(x,y,p)$, where p specifies the level in the normal direction in which the section is made. To demonstrate the use of projection and sections, we consider a (2×2) overlayer model system with an overlayer-substrate spacing of $d_s/2$, where d_s is the spacing between consecutive substrate layers. Using for illustrative purposes a s-wave scattering model[1] with scattering phase shifts $\delta_S=\pi/2$ and $\delta_o=\pi/8$ for the substrate and overlayer ion-cores, respectively, yields the kinematical intensity profiles of the (00) beam shown in Figs. 1(a) and 1(b) for the clean substrate (dashed) and overlayer system (solid). We note that for this configuration no new peaks occur (in the absence of multiple scattering), the profiles being different in line shape and relative intensities only.

In the following, we use the line projection $P^M(z)$, [Eq. (4)] which contains the projections of the interatomic vectors on the z axis, and the two-dimensional section $P(x,y,p)$ which contains the interatomic vectors between atoms at (x,y,z_1) and (x,y,z_2) where $p=z_1-z_2$, projected on the (xy) plane. The real part and modulus of the projection [see e.g. Eq. (4)] obtained by transforming the above overlayer intensity profile are shown in Figs. 1(d) and 1(f), respectively, while these for the clean surface are shown in Figs. 1(c) and 1(e). The expected locations of peaks are denoted by vertical arrows. It is seen that in both modes of the projection, peaks occur at $z\sim n(d_s/2)$ ($n=0$, 1, 2 ...) in the overlayer case, whereas in the transformation of the intensity profiles of the substrate, the maxima at odd values of n are missing, as expected. Attention is drawn to other peaks in the projection which are not associated with atomic locations in the model structure. These are data-truncation peaks and will be discussed in the next section. The ability to differentiate between different registries of the overlayer-substrate (overlayer atoms in twofold and fourfold sites) by the use of

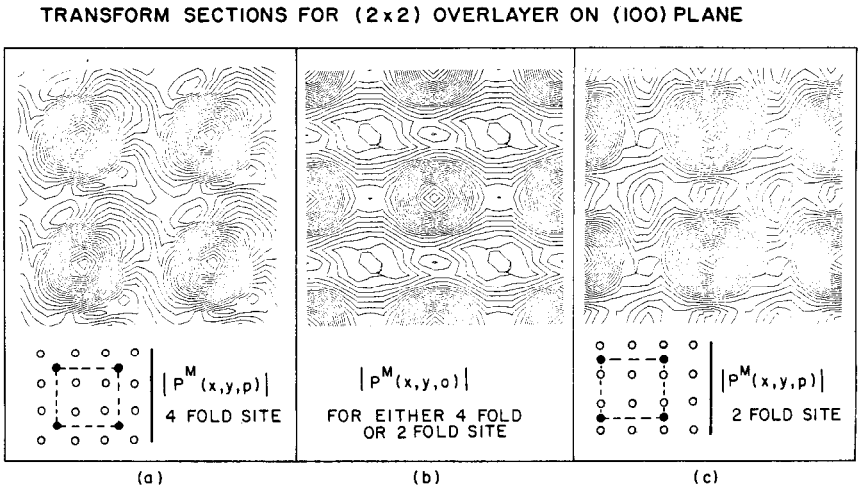

FIG. 2. Calculated transform sections for a (2×2) overlayer on the (100) face demonstrating the use of sections in the determination of overlayer-substrate registries. (a)—Transform section for an overlayer with atoms (solid circles) at the four-fold, high symmetry, sites with respect to the substrate net (open circles). The section was performed at the level $p=d_{so}=d_s/2$ given in Fig. 1(a). (b)—Transform section at the $p=0$ level for either the four-fold or two-fold site overlayer configuration. (c)—Transform section for an overlayer with atoms (solid circles) at the two-fold, bridge, sites with respect to the substrate net (open circles). The section was performed at the $p=d_{so}$ level. The above transform sections were calculated on the basis of kinematical intensity profiles of nine beams (h, $k=0$, 1, 2 indexed according to the substrate net), for the parameters specified in the caption to Fig. 1(a).

sections of the transform is demonstrated in Fig. 2. Sections at the level $n=d_s/2$, $[P(x,y,d_s/2)]$, for the two-fold and four-fold registries are shown in Figs. 2(a) and 2(c), respectively along with the $z=0$ section $[P(x,y,0)]$ in Fig. 2(b). These sections were derived from the specular and nonspecular diffracted beams [(h, $k=0$, 1, 2, indexed according to the substrate reciprocal net]. The $P(x,y,0)$ sections are essentially the same for both overlayer registries since this section contains projections of interatomic vectors between atoms located in the same (xy) plane (i.e., z level), whereas the $P(x,y,p)$ sections reflect different interlayer registries.

C. The Problem of Data Truncation

The extent and range of data is commonly a critical factor in the analysis of sampled experimental measurements. The particular problem in the application of transform methods to the analysis of LEED data is the finite number of diffraction beams and the finite range of their intensity profiles measured in the conventional LEED experiment. Since we have found empirically that reliable (xy) sections of the transform can be obtained using a rather small number of nonspecular diffraction beams [see e.g., discussion in the next section where the intensity profiles of the specular and three nonspecular measured diffraction beams are employed in deriving two-dimensional transform sections for the (100) face of Ni], we confine our discussion at this time to the effects of the finite range of the (00) beam intensity profiles on the transform analysis.

We define an ideal intensity profile for the application of our transform analysis, as shown in Fig. 3(a). This profile represents the contribution of the interference function including damping, to the kinematical intensity, i.e., the intensity of low-energy electrons diffracting kinematically from an ordered array of ion-core unit scatterers. This ideal intensity profile is periodic with peaks of constant amplitude, and extends to an infinite value of the normal momentum transfer variable. The $P^M(z)$ transform associated with the above profile is shown in Fig. 3(A) and consists of a periodic series of delta functions at positions corresponding to the projections on the z axis of all vectors between the ion-core unit scatterers.

Operationally a typical LEED measurement may be considered as viewing the above profile [Fig. 3(a)] through a data-window which affects the range and line shape of the record. Two possible data-windows are shown in Fig. 3(b). The window denoted by ω_1 is a box-car window which merely confines the range of the record, whereas the ω_2 window both limits the range of the record and also affects its line shape. This second window transforms the "ideal" interference function signal in Fig. 3(a) into the "realistic" profile shown in Fig. 3(c2). The truncation effect of the ω_1 window on the ideal signal is illustrated in Fig. 3(c1), where the ideal record [Fig. 3(a)] is terminated at some finite value S_M of the normal momentum transfer. The effect of multiplying the ideal intensity profile by the data windows, upon the transform of the products is shown in Figs. 3(C1) and 3(C2), where the modulus of the $P^M(z)$ projection for both profiles is given. Comparison of these results with the transform associated with the ideal signal [Fig. 3(A)] indicates that "windowing" the ideal profile results in a broadening of the delta functions and in the occurrence of additional peaks in the transform (Gibbs oscillations[8]), which are not directly related to the geometry of the array of ion-core scatterers.

From the above discussion, it is evident that a central problem in the extraction of structural information from transforms of LEED intensity profiles is the need to differentiate between peaks in the transform arising from the structural arrangement of the scattering centers and those arising from data truncation,[9] and

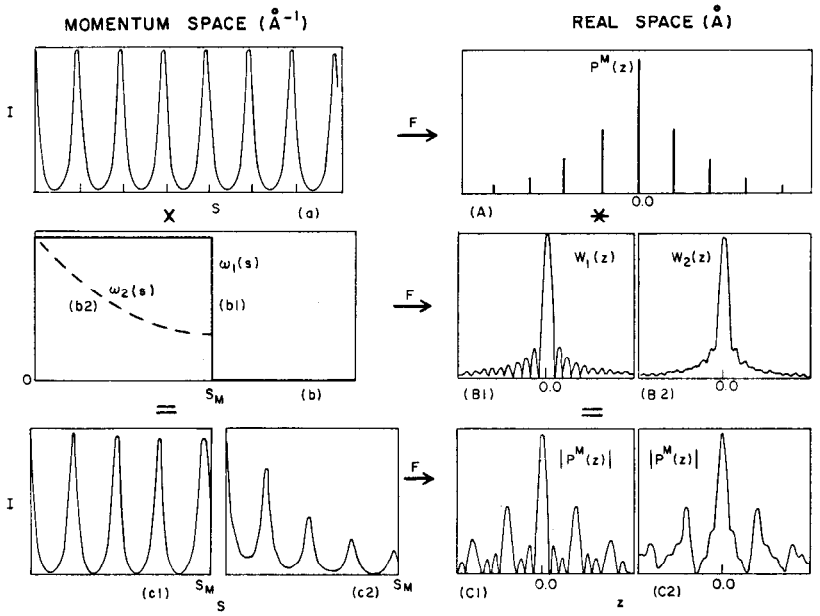

FIG. 3. Demonstration of the correspondence between momentum-space (S) operations and their transforms and the convolution in real space (z). (a)—The ideal profile representing the contribution of the interference function to the intensity. (A)—The transform corresponding to the profile shown in (a). (b)—Two typical data windows in momentum space. ω_1 is a box-car window which merely truncates the record at S_M, and ω_2 is a window which both truncates and also affects the line shape of the record. (B1) and (B2)—The spectral windows W_1 and W_2 corresponding to ω_1 and ω_2 in (b). Note the difference in main characteristics between the two. (c1) and (c2)—The resultant profiles obtained by multiplying the profile in (a) by ω_1 (c1), and ω_2 (c2), respectively. (C1) and (C2)—The modulus of the transform of the profiles shown in (c1) and (c2), respectively. Note the marked differences in line shapes between the two. As indicated in the figure these can be obtained by convoluting the delta function transform in (A) with the spectral windows in (B1) and (B2), respectively.

to precisely locate the "true" peaks. The solution to this problem arises from a consideration of the effects of data windows in real space, rather than as above in momentum space. This is achieved through application of the Convolution Theorem,[10] which may be written as

$$F[gh]=G*H, \tag{5}$$

where g and h are arbitrary functions, G and H are the transforms of g and h, respectively, F represents the Fourier transform operation, and "$*$" denotes the convolution operation. Thus, in the present context the transform of the multiplication of the ideal intensity profile [Fig. 3(a)] by a data window [Fig. 3(b)], $P^M{}_{\rm OBS}(z)$ [Figs. 3(C1)–3(C2)], is equivalent to a convolution in real space of the transform of the ideal profile, $P^M{}_{\rm DELT}(z)$ and the spectral window, W, i.e.,

$$P^M{}_{\rm OBS}(z)=P^M{}_{\rm DELT}(z)*W(z). \tag{6}$$

This point is illustrated in Fig. 3; convolution of the transforms, W_1 and W_2 [Figs. 3(B1) and 3(B2)] of the data windows ω_1 and ω_2, with the transform, $P^M{}_{\rm DELT}(z)$ [Fig. 3(A)] of the ideal profile yields the transform functions shown in Figs. 3(C1) and 3(C2), respectively.

Since by the convolution theorem $P^M{}_{\rm OBS}(z)$ in Eq. (6) is simply the transform of the *finite* intensity profile, the equation can be solved for $P^M{}_{\rm DELT}(z)$, if the data window ω, and hence its transform W, is known. Accordingly, we have constructed a transform-deconvolution procedure[11] which proceeds in the following steps.

1. The transform of the intensity data is performed.
2. A trial delta function transorm is constructed and its convolution with the appropriate spectral data window is calculated.
3. The fit between the observed transform obtained from step 1 and the calculated transform resulting from step 2 is determined.
4. Steps 2–3 are iterated until a best fit is obtained.

The final value of the delta function transform distinguishes the "true" peaks in the observed transform and their positions to a high degree of precision, as is demonstrated in the analysis of LEED intensity data from Ni(100) in the following section.

It is interesting to note at this point that an alternative method of suppressing the effects of data truncation has been suggested.[12] This consists of a multiplication in momentum space of the intensity profiles by a data window chosen to minimize the Gibbs oscillations in the transform. We have found that this procedure, using an appropriate window function,[13] can significantly attenuate the data truncation peaks, but only at the expense of a very considerable, and for our purposes, unacceptable loss of resolution in the transform. This effect can be readily understood by noting that the equivalent procedure in real space, by the convolution theorem, consists of a convolution of the transform of the data window with the transform of the intensity profile. In practice the spectral window (transform of the data-window) is chosen to minimize the side lobes of the function, in order to reduce the Gibbs oscillations, but this has as corollary the effect of broadening the main lobe, and consequently of further broadening the peaks in the transform of the intensity profile.

D. Geometrical Interpretation of the Transform

As we have noted in an earlier section, in the case of x-ray diffraction, the Patterson function [Eqs. (1) and (2)] represents the self-convolution of charge densities in the diffracting material, and is in principle a real, positive definite function. The transform that we have constructed for the LEED case [Eq. (3)] is a complex function. The main characteristics of LEED intensity profiles consist of peaks at positions corresponding to the satisfaction of the basic laws of diffraction, dressed by the effects of multiple scattering and details of the

scattering potential.[9] It can be shown easily that the square of the modulus of our transform is equal to the transform of the autocovariance function[14] of the intensity profile,

$$|P^M(z)|^2 = \int dS C(S) \exp[2\pi i S z], \tag{6}$$

where C is the autocovariance function defined as

$$C(\tau) = \int dS I_{00}(S) I_{00}(S+\tau). \tag{7}$$

By construction, the autocovariance of the intensity profile seeks and enhances periodic features in the intensity profile, and in addition, performs a local averaging in momentum space. Thus, the main maxima in the transform of the autocovariance function are associated with the above mentioned periodicities in the intensity profile dictated by the diffraction laws and the geometrical arrangement of the scatterers.

III. APPLICATION TO SURFACE STRUCTURAL DETERMINATION OF Ni(100)

Having discussed some principles of our transform method, we present in this section an application of the technique to the LEED data obtained by Demuth and Rhodin[4] for Ni(100). The intensity profiles for the specularly diffracted beam for various angles of incidence are shown in Fig. 4(b). These profiles exhibit strong dynamical characteristics and extend over a range of ~10–240 eV.

The transform projections obtained from the above profiles, together with the transform result for the angle averaged intensity curve are shown in Fig. 4(a). We note that for this system there is no marked improvement achieved in the real part of the transform by angular averaging. The resulting values for the layer spacing based on the individual profiles are in the range of 1.76–1.81 Å, in excellent agreement with the x-ray bulk value of 1.76 Å. As an illustration of the use of the deconvolution procedure, we include also in Fig. 4(a) the convoluted-delta-function best fit to the transform of the $\theta = 12°$ intensity profile. The best-fit result for the layer spacing is 1.78 Å as compared to a peak in the transform of the $\theta = 12°$ profile at 1.80 Å.

A complete determination of the structure was achieved by calculating two-dimensional sections of the transform, using the above specular diffraction profiles and the intensity data for the (01), (10), and (11) diffracted beams which were measured[4] for an azimuthal angle $\psi = 0°$, and polar angles of incidence $\theta = 0°$ for the (10) and (11) beams, and $\theta = -2°$ to 2° (in steps of 1°) for the (01) beam. The resulting sections are shown in Figs. 4(c) and 4(d) for the levels $p = 0$ Å, $[P^M(x,y,0)]$, and $p = 1.78$ Å, $[P^M(x,y,1.78\text{ Å})]$, respectively. These sections exhibit the expected characteristics of the interlayer and intralayer registry in the (100) plane and enable the determination of the lateral and vertical location of atoms in the surface layers to an accuracy of better than 5%.

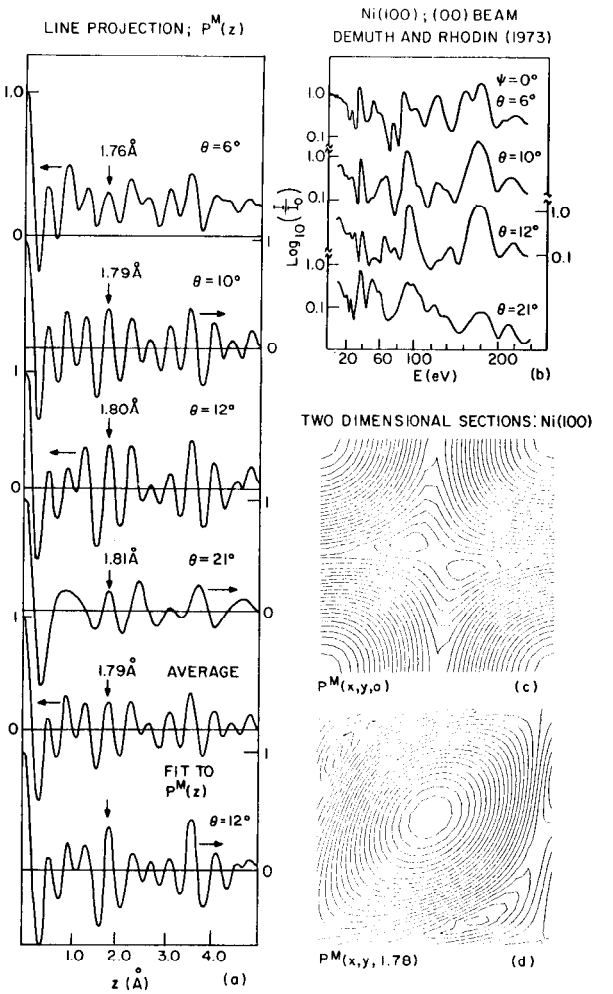

FIG. 4. Experimental intensity data and transform projections and sections for Ni(100). (a) Line transform projections, $P^M(z)$, normalized to unity derived from the intensity data shown in (b). The four top curves are the real parts of the transform projections of the individual (00) intensity profiles. Vertical arrows indicate location of peaks ranging between 1.76–1.81 Å. The curve-marked average was obtained by transforming the angular averaged profile of the intensities shown in (b). The fit to the $\theta = 12°$ transform, shown at the bottom, was obtained according to the transform deconvolution procedure outlined in the text with the best-fit delta-function profile $[P^M{}_{\text{DELT}}(z)$ in Eq. (6)] having peaks at $z = 0$, 1.78, and 3.56 Å only. All other peaks in the fit, and thus in the reference $\theta = 12°$ transform, result from the convolution with the spectral window. Thus the method allows for distinguishability between true- and data-truncation peaks as well as precise determination of the layer spacings. (b)—Measured intensity profiles[4] of the (00) diffracted beam from Ni(100) with azimuthal angle $\psi = 0°$, and four polar angles of incidence $\theta = 6°$, 10°, 12°, and 21°. Note the strong dynamical features in the profiles. (c) and (d)—Two-dimensional transform sections obtained from the specular diffractions shown in (b) and three measured[4] nonspecular beams: (10) and (11) with $\theta = \psi = 0°$ and (01) with $\psi = 0°$ and $\theta = -2°$ to 2° (in steps of 1°). Despite the small number of available beams, the peaks at the corners of the $P^M(x,y,0)$ section (c) and the center peak in the $P^M(x,y,1.78)$ section (d), exhibit unambiguously the registry in the (100) face.

IV. SYNOPSIS

In conclusion, we have outlined in this paper the principles of our transform-deconvolution method for the determination of surface structures from LEED data. We have demonstrated the application of the

method to the complete determination of the surface structure of Ni(100) from experimental data. The method is currently being used for the determination of the atomic arrangements in both clean and overlayer systems.[15]

ACKNOWLEDGMENTS

The authors are indebted to the staff of the Sigma-7, Rochester Technical Computer Center, in particular Donald D. Smith and Richard R. Bergan, and to John E. Klock and Paul R. Pellika of the Art Services for their invaluable cooperation and help. Mrs. Carol Troy is gratefully acknowledged for her assistance in the preparation of the manuscript.

[1]C. B. Duke in *LEED-Surface Structure of Solids*, Part II, edited by M. Laznička (Union of Czechoslovak Mathematicians and Physicists, Prague, 1972).
[2]D. W. Jepsen, P. M. Marcus, and F. Jona, Phys. Rev. **B5**, 3933 (1972).
[3]S. Anderson and J. B. Pendry, J. Phys. C **6**, 601 (1973).
[4]J. E. Demuth and T. N. Rhodin (to be published).
[5](a) A. Guinier, *X-ray Diffraction* (W. H. Freeman, San Francisco, 1963); (b) H. Lipson and W. Cochran, *The Determination of Crystal Structures* (G. Bell, London, 1966), Chap. 7.
[6]M. J. Buerger, *Vector Space* (J. Wiley, New York, 1959).
[7](a) T. A. Clarke, R. Mason, and M. Tescari, Surface Sci. **30**, 553 (1972); (b) T. A. Clarke, R. Mason, and M. Tescari, Proc. Roy. Soc. Lond. **A331**, 321 (1972).
[8]C. Lanczos, *Applied Analysis* (Prentice Hall, New York, 1966), Chap. IV.
[9]Multiple-scattering features in the intensity profiles do not alter the characteristics of our transform-deconvolution technique and its general method of application. Analysis of the experimental intensity data for Ni(100) proved to be successful despite the marked dynamical structure of the measured intensity profiles (see e.g., Sec. III). This conclusion derives in part from the smoothing characteristics of the autocovariance function (see Sec. IID). In some cases it might be advantageous to use angular averages of the diffracted beams, including in the averaging a rather small number of intensity profiles which span a wide range of incidence angles. Details of this study will be reported elsewhere (U. Landman and D. L. Adams, to be published).
[10]R. Hoseman and S. N. Bagchi, *Direct Analysis of Diffraction by Matter* (North-Holland, Amsterdam, 1962).
[11]Alternative methods of deconvolution using Laplace transformation and matrix inversion are under study.
[12]M. G. Lagally (private communication).
[13](a) J. F. Kaiser in *System Analysis by Digital Computer*, edited by F. F. Kuo and J. F. Kaiser (J. Wiley, New York, 1966); (b) G. B. Bergland, IEEE, Spectrum **6**, 41 (1969).
[14]R. B. Blackman and J. W. Tukey, *The Measurement of Power Spectra* (Dover, New York, 1959).
[15]D. L. Adams and U. Landman (to be published).